Pressure dependence of the low-temperature crystal structure and phase transition behavior of CaFeAsF and SrFeAsF: A synchrotron x-ray diffraction study

S. K. Mishra,[1] R. Mittal,[1,*] S. L. Chaplot,[1] S. V. Ovsyannikov,[2] D. M. Trots,[2] L. Dubrovinsky,[2] Y. Su,[3] Th. Brueckel,[3,4] S. Matsuishi,[5] H. Hosono,[5] and G. Garbarino[6]

[1]*Solid State Physics Division, Bhabha Atomic Research Center, Trombay, Mumbai 400 085, India*

[2]*Bayerisches Geoinstitut, Universitat Bayreuth, Universitatsstrasse 30, D-95440 Bayreuth, Germany*

[3]*Juelich Centre for Neutron Science, IFF, Forschung. Juelich, FRM II, Lichtenbergstr. 1, D-85747 Garching, Germany*

[4]*Institut fuer Festkoerperforschung, Forschungszentrum Juelich, D-52425 Juelich, Germany*

[5]*Frontier Research Center, Tokyo Institute of Technology, 4259 Nagatsuta-cho, Midori-ku,Yokohama 226-8503, Japan*

[6]*European Synchrotron Radiation Facility, BP 220, 38043 Grenoble, France*

(Received 9 May 2011; revised manuscript received 5 August 2011; published 21 December 2011)

We report systematic investigation of high pressure crystal structures and structural phase transition up to 46 GPa in CaFeAsF and 40 GPa in SrFeAsF at 40 K using powder synchrotron x-ray diffraction experiments and Rietveld analysis of the diffraction data. We find that CaFeAsF undergoes orthorhombic to monoclinic phase transition at $P_c = 13.7$ GPa while increasing pressure. SrFeAsF exhibits coexistence of orthorhombic and monoclinic phases over a large pressure range from 9 to 39 GPa. The coexistence of the two phases indicates that the transition is of first order in nature. Unlike in the 122 compounds ($BaFe_2As_2$ and $CaFe_2As_2$), we do not find any collapse tetragonal transition. The transition to a lower symmetry phase (orthorhombic to monoclinic) in 1111 compounds under pressure is in contrast with the transition to a high symmetry phase (orthorhombic to tetragonal) in 122-type compounds. On heating from 40 K at high pressure, CaFeAsF undergoes monoclinic to tetragonal phase transition around 25 GPa and 200 K. Further, it does not show any post-tetragonal phase transition and remains in the tetragonal phase up to 25 GPa at 300 K. The dP_c/dT is found to be positive for the CaFeAsF and $CaFe_2As_2$, however the same was not found in case of $BaFe_2As_2$.

DOI: 10.1103/PhysRevB.84.224513 PACS number(s): 74.70.−b, 61.50.Ks, 72.80.Ga

I. INTRODUCTION

Crystal structures and phase transitions are vital to superconductivity in iron-based compounds.[1–20] These compounds occur in five different structural classes[2] (namely, FeSe, LiFeAs, $BaFe_2As_2$, LaFeAsO/SrFeAsF, and $Sr_3Sc_2O_5Fe_2As_2$) but share a common layered structure based on a planar layer of iron atoms joined by tetrahedrally coordinated pnictogen (Pn = P, As) or chalcogen (S, Se, Te) anions arranged in a stacked sequence separated by alkali, alkaline-earth, or rare-earth (Ba, Ca, Sr, Eu) and oxygen/fluorine blocking layers. It is now widely thought that the interaction that leads to the high T_c superconductivity originates within these common iron layers, similar in nature to the common copper oxygen building block found in the copper oxide (cuprate). However, structurally three key differences are found among the FeAs and cuprate compounds. First, in the FeAs compounds the pnictogen/chalcogen anions are placed above and below the planar iron layer as opposed to the planar copper-oxygen structure of the cuprates. Second, ability to substitute or dope directly into the active pairing layers of FeAs compounds and finally the parent compounds of the new Fe-based superconductors share a similar electronic structure with all five d orbitals of the Fe contributing to a low density of states at the Fermi level, which is in contrast to the cuprates where parent compounds are Mott insulators with well-defined local magnetic moments. These similarities have inspired a flurry of theoretical and experimental works[1–30] in Fe pnictides-based materials.

At ambient condition, these compounds crystallize in tetragonal symmetry with no magnetic order (i.e., paramagnetic in nature). The parent compounds of iron-pnictides undergo a first- or second-order structural transition below room temperature (typically in the range of 100–210 K), from tetragonal to orthorhombic structure, and magnetic transition from nonmagnetic to stripe antiferro-magnetic structure.[2–7,22,24,29,30] The structural transition and magnetic ordering can happen simultaneously or successively depending on the compound. It has been confirmed both experimentally and theoretically that the magnetic order of Fe at low temperature is stripelike antiferromagnetism often referred to as spin density wave (SDW).[2–7] Upon changing the carrier concentration, applying external pressure or by charge neutral doping, the magnetic order suppresses, and the materials become superconducting. In the 1111-family (both RFeAsO and MFeAsF, R = rare earth and M = Ca and Sr), magnetic transition temperature (T_N) is lower than structural transition temperature (T_S). This seems to suggest that the magnetic transition is induced by the structural transition. In case of $M'Fe_2As_2$ (M′ = Ba, Sr, Ca, and Eu) compounds, (at ambient pressure with decreasing temperature) the structural and magnetic transitions are found[29,30] to happen simultaneously (a first-order transition). However, recent high pressure powder x-ray synchrotron diffraction studies on $BaFe_2As_2$ show that at low temperature (33 K), these transitions occur at different pressures.[19] It is not clear whether the magnetic transition is induced by the structural transition and what is the driving force of the structural transition. These two important questions are crucial to understand the formation of the stripe antiferromagnetic order in the parent compounds.

The magnetism is intimately related to the crystal structure both in terms of the Fe-As bond length and As-Fe-As bond angle. The antiferromagnetic ordering can be suppressed by

various ways such as by changing the carrier concentration, applying external pressure, or by charge neutral doping. The common FeAs building block is considered as a critical component to stabilize superconductivity. The combination of strong bonding between Fe-Fe and Fe-As sites (and even interlayer As-As in the 122-type systems), and the geometry of the $FeAs_4$ tetrahedra plays a crucial role in determining the electronic and magnetic properties of these compounds. For instance, the two As-Fe-As tetrahedral bond angles seem to play a crucial role in optimizing the superconducting transition temperature. The highest T_c values are found only when an As-Fe-As/Fe-As-Fe tetrahedral bond angle is close to the ideal value of 109.47°. The detailed interplay between the crystal structure, magnetic ordering, and superconductivity is hardly understood.

High pressure experiments play an important role in the field of superconductivity and also provide information about the understanding of its mechanism. The superconducting transition temperature (T_c) in FeAs compounds is found to increase[14–21] over 50 K by application of pressure. Despite the importance of the evolution of superconducting transition temperature (T_c) with pressure to understand the mechanism of superconducting properties of Fe-based materials, there is lack of information on the detailed pressure dependence of their structural properties. Recently, we reported the pressure effects on $CaFe_2As_2$ and $BaFe_2As_2$ (122-type compounds) using powder synchrotron x-ray diffraction technique. Rietveld analysis of the high pressure powder x-ray diffraction data showed[19] that at 300 K in the Ba-compound the collapsed tetragonal transition occurs at 27 GPa. The transition pressure value is found to be much higher as compared to the Ca-compound where the transition occurs at 1.7 GPa. However, at low temperature (33 K), structural phase transition from the orthorhombic to tetragonal phase in the Ba-compound occurred at about 29 GPa (while increasing pressure), which is much higher than the transition pressure of 0.3 GPa at 40 K, as known in case of the Ca-compound.[19] We have not found any evidence of a post collapsed tetragonal phase transition in $CaFe_2As_2$ up to 51 GPa (at 300 K) and 37.8 GPa (at 40 K). It is important to note that transition to a collapsed phase occurs in the two compounds at nearly the same values of unit cell volume and c_t/a_t ratio. Although five different types[2] of Fe-based superconductors have been reported in literature, the 122 FeAs-based superconductors seem to be the most studied (of the five types). On the other hand 1111-type compounds have not gotten considerable attention from the scientific community. In this paper we present systematic investigation of pressure effect on crystal structure, and structural phase transition behavior of CaFeAsF and SrFeAsF at 40 K using powder-diffraction technique. Detailed Rietveld analysis of the diffraction data shows that both the compounds undergo a structural phase transition from orthorhombic to monoclinic phase on compression. While CaFeAsF undergoes a fairly sharp transition at around 13.7 GPa, SrFeAsF exhibits a large phase coexistence region (from 9 to 40 GPa) with the orthorhombic phase fraction continuously decreasing with increase of pressure. Possible correlation between structure evolutions with pressure and superconductivity in Fe-based superconductor is also discussed.

II. EXPERIMENTS

The pressure-dependent powder x-ray diffraction measurements were carried out using the ID-27 beam line at the European Synchrotron Radiation Facility (ESRF, Grenoble, France). An applied pressure was generated by membrane diamond anvil cells (DACs). We employed a stainless steel gasket preindented to the thickness of ~40–50 μm, with a central hole of 150 μm in diameter and filled with helium as pressure transmitting media. The pressure was determined from the shift of the fluorescence line of the ruby. A powdery sample of ~30–40 μm in diameter and 10 μm in thickness was situated in the center of one of the diamond anvil's tips. The wavelength of the x-ray (0.3738 Å) was selected and determined using a Si(111) monochromator and the iodine K-edge. The sample-to-image plate (MAR345) detector distance was refined using the standard diffraction data of Si. To cool the DAC, a continuous helium flow CF1200 DEG Oxford cryostat was used. Precaution was taken to obtain stable temperature and pressure conditions prior to each acquisition. The precision

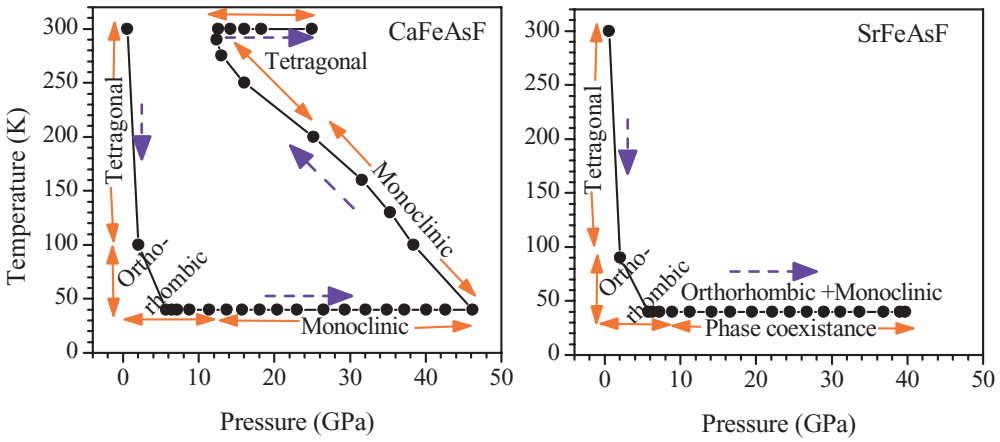

FIG. 1. (Color online) The pressure-temperature path (indicated by blue, dashed line and arrows) as followed in our measurements on CaFeASF and SrFeAsF. Symbols correspond to the pressure-temperature conditions where measurements were made. The solid lines through the symbols are a guide to the eye. The phases, namely tetragonal, orthorhombic, and monoclinic, as identified by Rietveld refinement of the diffraction data are indicated over ranges shown by red lines and arrows.

and accuracy of the temperature measurement is better than 0.1 K and 0.2 K, respectively. During the measurements, the CaFeAsF and SrFeAsF samples were first cooled to 40 K, and then pressure was increased along a path indicated in Fig. 1. Typical exposure times of 20 seconds were employed for the measurements. Preferred orientation of crystal grains is observed along different axes in different loadings, which is common in high-pressure experiments. The diffraction patterns indicate preferred orientation of the samples along [211] and [132] for measurements on CaFeAsF and SrFeAsF, respectively.

The two-dimensional (2D) powder images were integrated using the program FIT2D[31] to yield intensity vs 2θ plot. The structural refinements were performed using the Rietveld refinement program FULLPROF.[32] In all the refinements the background was defined by a sixth-order polynomial in 2θ. A Thompson-Cox-Hastings pseudo-Voigt with axial divergence asymmetry function was chosen to define the profile shape for the powder synchrotron x-ray diffraction peaks. The scale factor, background, and half-width parameters, along with mixing parameters, lattice parameters, and positional coordinates, were refined.

III. RESULT AND DISCUSSION

The powder synchrotron x-ray diffraction measurements for MFeAsF (M = Ca, Sr) at ambient conditions confirmed single-phase samples consistent with the published reports.[22,24–26] The effects of pressure inhomogeneity on the phase transition behavior of FeAs-based compounds have been reported in literature.[14–19] In the present measurements we have used helium as a pressure transmitting medium, which is believed[33] to give the best hydrostatic conditions at present. However, effect of inhomogeneity could not be completely ruled out and could have some influence on the results obtained on these compounds.

A. Phase transition of CaFeAsF at 40 K

At ambient condition, CaFeAsF crystallizes in tetragonal structure with space group $P4/nmm$ without magnetic ordering. On cooling it undergoes a tetragonal to orthorhombic phase transition at 134 K, while magnetic ordering in the form of a SDW sets in at around 114 K, respectively. Figures 2(a) and 2(b) show a Rietveld refinement of powder synchrotron data at 300 K (0.6 GPa) and at 40 K (5.8 GPa), respectively. Splitting of $(220)_T$ peak of tetragonal phase at 300 K unambiguously confirms the orthorhombic structure at 40 K (see inset).

The pressure-dependent powder x-ray diffraction measurements were carried out at 40 K and at pressures between 5.8 to 46.2 GPa. The data show significant changes with pressure especially in terms of dissimilar broadening of various peaks. The most prominent changes have been observed in peaks around $2\theta = 11^\circ$, which become broader with increasing pressure above 12 GPa. Figure 3 depicts a portion of the powder

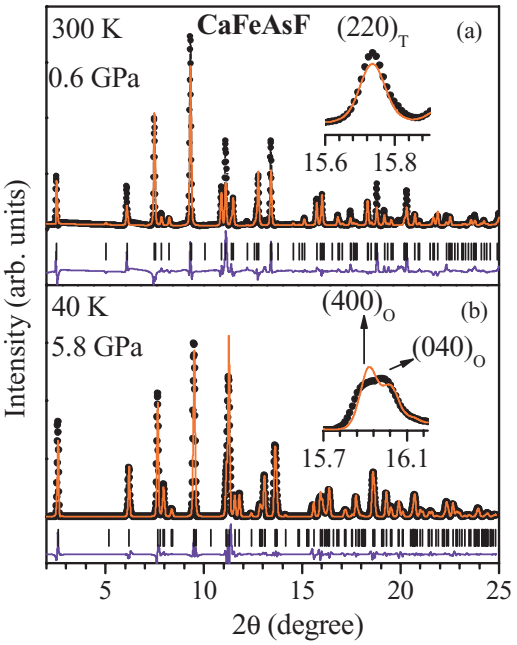

FIG. 2. (Color online) Observed (solid black circles), calculated (continuous red/dark gray line), and difference (bottom blue/medium gray line) profiles obtained after the Rietveld refinement of CaFeAsF at (a) 0.6 GPa and 300 K in tetragonal phase (space group $P4/nmm$) and (b) 5.8 GPa and 40 K in orthorhombic phase (space group $Cmma$). Inset in (a) shows the (220) reflection of the tetragonal phase and in (b) shows the splitting/broadening of the (220) reflection of the tetragonal phase at 40 K and provides unambiguous signature for orthorhombic structure.

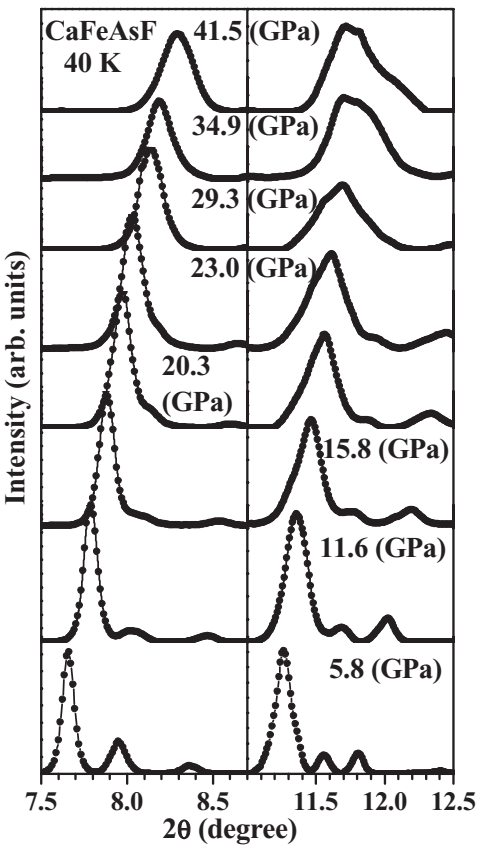

FIG. 3. Evolution of the powder-synchrotron x-ray diffraction patterns of CaFeAsF at 40 K and selected pressure.

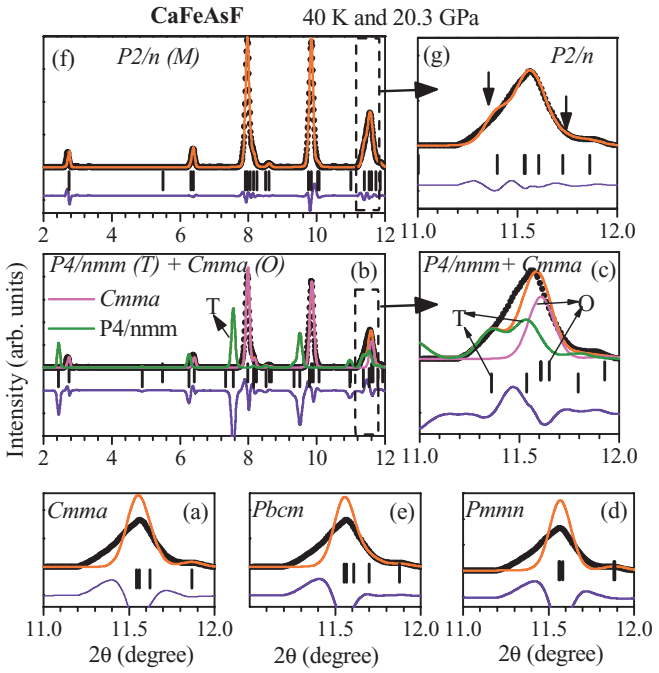

FIG. 4. (Color online) Observed (solid black circles), calculated (continuous red/dark gray line), and difference (bottom blue/medium gray line) profiles obtained after the Rietveld refinement of CaFeAsF at 40 K and 20.3 GPa using different models, namely (a) an orthorhombic (*Cmma*); (b), (c) a combination of tetragonal ($P4/nmm$) and an orthorhombic (*Cmma*); (d), (e) an orthorhombic (*Pmmn*, *Pbcm*); and (f), (g) monoclinic ($P2/n$) phases, respectively.

x-ray diffraction patterns of CaFeAsF at selected pressure. Detailed Rietveld refinement of the powder-diffraction data shows that diffraction patterns at 40 K could be indexed using the orthorhombic structure (space group *Cmma*) up to 12 GPa. The Rietveld refinements proceeded smoothly, revealing a monotonic decrease in lattice constant and cell volume with increasing pressure. The response of structural parameters to pressure is strongly anisotropic (as will be shown below in Fig. 9). Further increase of pressure above 12 GPa leads to even higher compression of the interlayer spacing (lattice parameter *c*). However, attempts to employ the same orthorhombic structural model in the refinements [Fig. 4(a)] proved unsatisfactory, and a progressive worsening of the quality of the Rietveld fits with increasing pressure was found. The most apparent signature of the subtle structural transformation that occurs above 12 GPa is the inability of orthorhombic structure (space group *Cmma*) to account satisfactory for the peaks around 11°. For more clarity it is shown in Fig. 4(a) that the diffraction data at 20.3 GPa cannot be indexed with the orthorhombic phase. Extra broadening (splitting) of peaks suggests either lowering of the symmetry or coexistence of another high symmetry phase.

Recently, we reported in $BaFe_2As_2$ compounds that low temperature orthorhombic (space group *Fmmm*) and room temperature tetragonal (space group $I4/mmm$) phases coexist over a large pressure range above 29 GPa.[19] In view of this, to account for the peak broadening in the pressure-dependence diffraction data on CaFeAsF, we have explored the possibility of coexistence of low temperature orthorhombic (space group *Cmma*) and room temperature tetragonal (space group $P4/nmm$) phases. The powder-diffraction data above 12 GPa are refined using these coexisting phases, and the results are shown in Figs. 4(b) and 4(c). The green color line (online only and marked with T) represents the additional tetragonal phase. While the profile around 11.5° could be

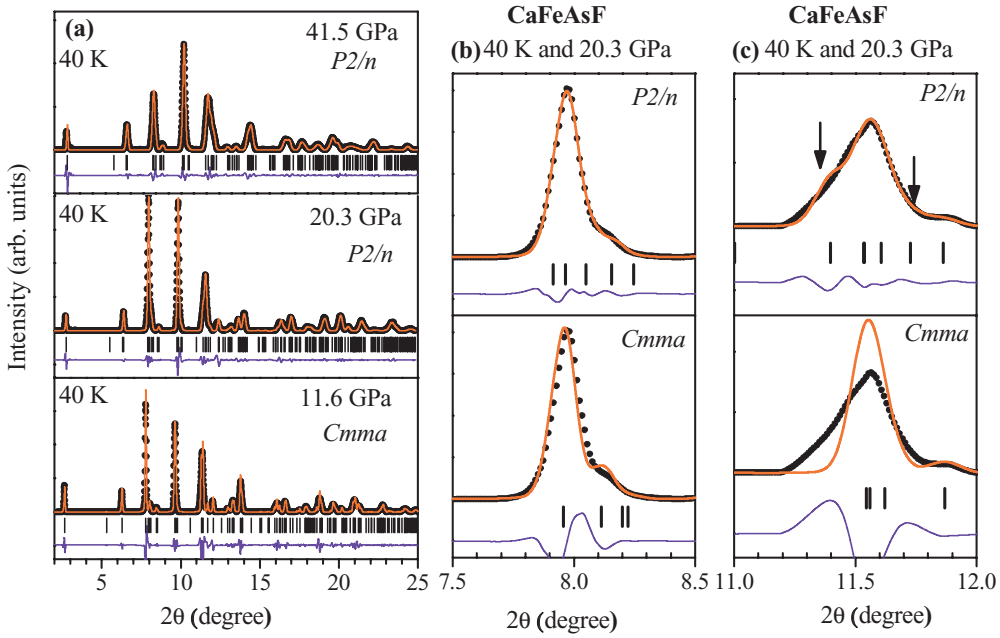

FIG. 5. (Color online) (a) Observed (solid black circles), calculated (continuous red/dark gray line), and difference (bottom blue/medium gray line) profiles obtained after the Rietveld refinement of CaFeAsF at selected pressures and 40 K. The diffraction profiles at 11.6 GPa are refined using an orthorhombic (*Cmma*) phase, while the profiles at 20.3 and 41.5 GPa are refined monoclinic ($P2/n$) phase. (b), (c) The refinement of the diffraction pattern at 20.3 GPa and 40 K with an orthorhombic phase (space group *Cmma*) and monoclinic ($P2/n$) phase.

TABLE I. Results of Rietveld refinement of the crystal structure for CaFeAsF at selected pressure and 40 K. The measurements were carried out using a focused x-ray monochromatic beam of wavelength = 0.3738 Å. The data collected up to 25° have been used to determine the reported parameters. The atomic positions for space group *Cmma* (No. 67): Ca (4g)(0, 1/4, *z*), Fe (4b) (1/4, 0, 1/2), As (4g) (0, 1/4, *z*) and F (4a) (1/4, 0, 0). The atomic positions for space group $P12/n1$ (No. 13, unique axis *b* and cell choice 2): Ca (2f)(3/4, *y*, 1/4), Fe (2e) (3/4, *y*, 3/4), As (4g) (3/4, *y*, 1/4), and F (4a) (3/4, *y*, 3/4).

	At 5.72 GPa and 40 K			29.3 GPa and 40 K		
	Orthorhombic phase (space group *Cmma*)			Monoclinic phase (space group $P12/n1$)		
Atoms	Positional coordinates			Positional coordinates		
	X	*Y*	*Z*	*X*	*Y*	*Z*
Ca	0	1/4	0.1640(1)	3/4	0.1750(2)	1/4
Fe	1/4	0	0.5000	3/4	0.4892(1)	3/4
As	0	1/4	0.6618(6)	3/4	0.6639(3)	1/4
F	1/4	0	0.0000	3/4	−0.0493(4)	3/4
Lattice parameters						
a (Å)		5.4012(1)		3.6733(2)		
b (Å)		5.3733(2)		7.5810(2)		
c (Å)		8.2897(3)		3.7156(2)		
				$\beta = 90.83\ (3)^\circ$		
$R_p = 14.5$; $R_{wp} = 25.7$; $R_{exp} = 13.34$; $\chi^2 = 3.71$				$R_p = 17.8$; $R_{wp} = 23.4$; $R_{exp} = 13.39$; $\chi^2 = 3.05$		

fitted (forcefully), the calculated peaks around 2.5°, 7.9°, and 9.8° arising due to the tetragonal phase are not observed in the experiments. This unsatisfactory quality of the Rietveld fit of the diffraction data suggests that the possibility of the phase coexistence of orthorhombic and tetragonal phases is not favored. The dissimilar broadening of peaks and inability to Rietveld fit the powder-diffraction patterns using a phase-coexistence model suggests a reduction of symmetry from the orthorhombic symmetry (space group *Cmma*).

We have further explored various possibilities, namely, orthorhombic symmetry with space group *Pbcm* and *Pmmn*, monoclinic structure with space group $P12/n1$, etc. [see Figs. 4(d)–4(g)], to identify the correct space group. We found that orthorhombic space groups (*Pbcm*, *Pmmn*) also could not fit structural data very well, and the monoclinic structure with space group $P12/n1$ (No. 13, unique axis *b* and cell choice 2) could successfully index all the peaks [see Figs. 4(f) and 4(g)]. It is well documented in literature that many isostructural Fe-based materials undergo a structural phase transition to the monoclinic phase with temperature and pressure.[34,35] Rietveld refinements employing this structural model are satisfactory for all the diffraction patterns up to the highest pressure measured by us. A careful inspection and analysis of diffraction data reveal that CaFeAsF transforms to the monoclinic structure at $P_c = 13.7$ GPa even though the monoclinic distortion is quite small. The monoclinic angle as a function of pressure shows a sharp discontinuity at the transition pressure at 13.7 GPa. The monoclinic angle (β) shows a very small change from 90.5° to 91.2° on increase in pressure from 13.7 GPa to 46.2 GPa. However, the small monoclinicity has significantly improved the fit quality between the observed and calculated profiles, as shown in Fig. 5. The detailed structural parameters and goodness of fit for CaFeAsF at selected pressure and 40 K, as obtained from powder-synchrotron diffraction data, are given in Table I. Schematic diagrams of the crystal structure in the orthorhombic and monoclinic phases are shown in Fig. 6.

B. Phase transition of SrFeAsF at 40 K

SrFeAsF also crystallizes in tetragonal structure with space group $P4/nmm$ at ambient condition. On cooling it undergoes a structural phase transition to orthorhombic phase around 180 K, followed by paramagnetic to antiferromagnetic

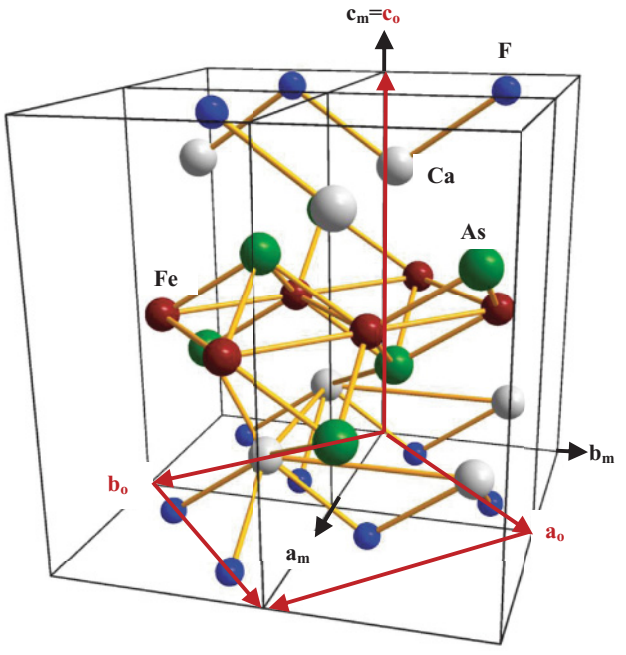

FIG. 6. (Color online) The relation between the unit-cell parameter of the low pressure orthorhombic phase and that of the high pressure monoclinic phase. a_o, b_o, c_o, and a_m, b_m, and c_m are cell edges in the orthorhombic and monoclinic phases, respectively. The relationship between the unit-cell parameter in the orthorhombic and monoclinic phases can be approximately described as $\mathbf{a_o} = \mathbf{a_m} + \mathbf{b_m}$, $\mathbf{b_o} = \mathbf{a_m} - \mathbf{b_m}$, $\mathbf{c_o} = \mathbf{c_m}$. The colored solid circles represent the atoms: Ca, white; Fe, red/dark gray; As, green/gray; and F, blue/medium gray in the unit cell.

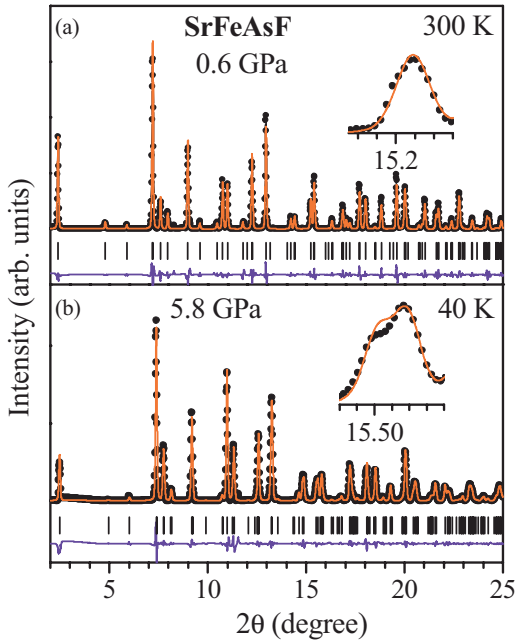

FIG. 7. (Color online) Observed (solid black circles), calculated (continuous red/dark gray line), and difference (bottom blue/medium gray line) profiles obtained after the Rietveld refinement of SrFeAsF at (a) 0.6 GPa and 300 K in tetragonal phase (space group $P4/nmm$) and (b) 5.8 GPa and 40 K in orthorhombic phase (space group $Cmma$). Inset in (a) shows the (220) reflection of the tetragonal phase and in (b) shows the splitting/broadening of the (220) reflection of the tetragonal phase at 40 K and provides unambiguous signature for orthorhombic structure.

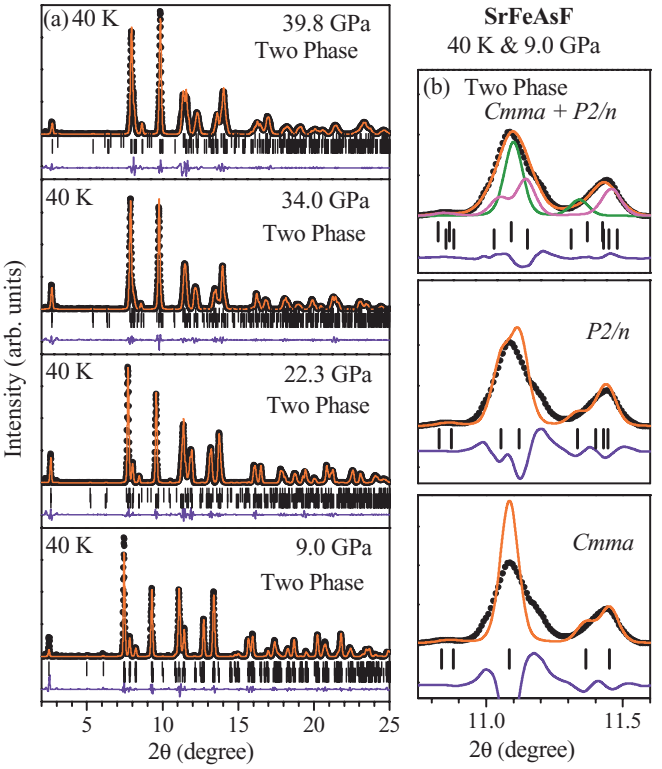

FIG. 8. (Color online) (a) Observed (solid black circles), calculated (continuous red/dark gray line), and difference (bottom blue/medium gray line) profiles obtained after the Rietveld refinement of SrFeAsF at selected pressures and 40 K. The diffraction profiles at 9.0, 22.3, 34.0, and 39.8 GPa are refined using a combination of orthorhombic ($Cmma$) and monoclinic ($P2/n$) phases. Upper and lower vertical tick marks above the difference profiles indicate peak positions of orthorhombic ($Cmma$) and monoclinic ($P2/n$) phases, respectively. (b) The refinement of the diffraction pattern at 9.0 GPa and 40 K with an orthorhombic phase (space group $Cmma$), a monoclinic ($P2/n$) phase, and a combination of orthorhombic (space group $Cmma$) and monoclinic ($P2/n$) phases.

transition at 133 K. Figures 7(a) and 7(b) depict results of Rietveld refinement of powder synchrotron data at 0.6 GPa and 300 K and 5.8 GPa and 40 K, respectively. At low temperature, we found that refinement for SrFeAsF can be carried out in the orthorhombic structure consistent with literature. The observation is unambiguously confirmed by comparing the $(220)_T$ peak of tetragonal phase at ambient temperature (see inset).

As in the case of CaFeAsF, the powder-diffraction patterns of SrFeAsF also show significant changes with pressure. To obtain the pressure dependence of the structural parameters, detailed Rietveld refinement of the powder-synchrotron x-ray diffraction data are carried out. Similar to CaFeAsF, we notice broadening/splitting of some of the peaks around 9 GPa. At this pressure, the diffraction data could not be refined using either the orthorhombic or the monoclinic phase, as indicated in Fig. 8. However, a two-phase refinement with both the orthorhombic and monoclinic space groups is found successful, and all the observed diffraction peaks could be indexed (see Fig. 8).

We find that orthorhombic and monoclinic phases coexist over a large pressure range from 9 GPa to the highest pressure of 40 GPa attained in our experiment. The percentage of the monoclinic phase continuously increases with pressure and reaches 98% at 40 GPa. The coexistence of both the phases indicates that the structural phase transition from orthorhombic to monoclinic phase is of first order. The fit between the observed and calculated profiles is quite satisfactory, and some of them are shown in Fig. 8. The detailed structural parameters and goodness of fit for SrFeAsF at selected pressure and 40 K, as obtained from powder-synchrotron diffraction data, are given in Table II.

In our earlier measurements for $BaFe_2As_2$ we found that the coexisting region for orthorhombic and tetragonal phase was very large.[19] In the case of the fluorine-based 1111-type Ca/Sr compounds the transition pressures are found to be very similar. These observations are in contrast to the case of $BaFe_2As_2$ and $CaFe_2As_2$, where the compound with smaller ionic radii ($CaFe_2As_2$) show phase transition at much lower pressure (0.3 GPa) at 40 K as compared to the $BaFe_2As_2$, where transition at 40 K occurs at 29 GPa.[19]

C. Pressure evolution of structural parameters at 40 K

As mentioned previously, superconductivity in iron-arsenide materials is associated with lattice distortion and suppression of magnetic ordering.[19,36,37] The detailed interplay between the crystal structure, magnetic ordering, and superconductivity is hardly understood up to now, which is to some extent due to the lack of precise structural data.

TABLE II. Results of Rietveld refinement of the crystal structure for SrFeAsF at selected pressure and 40 K. The measurements were carried out using a focused x-ray monochromatic beam of wavelength = 0.3738 Å. The data collected up to 25° have been used to determine the reported parameters. The atomic positions (Wycoff) for both the space groups are the same as given in Table I.

	At 5.8 GPa and 40 K			22.1 GPa & 40 K		
	Orthorhombic phase space group *Cmma*			Two phase: orthorhombic + monoclinic space group (*Cmma* + $P12/n1$)		
Atoms	Positional coordinates			Positional coordinates		
	X	*Y*	*Z*	*X*	*Y*	*Z*
Sr	0	1/4	0.1570(1)	0/0.75	0.25/0.1455(3)	0.1707(2)/0.25
Fe	1/4	0	0.5000	0.25/0.75	0/0.5131(1)	0.5/0.75
As	0	1/4	0.6602(6)	0/0.75	0.25/0.6703(2)	0.6606(5)/0.25
F	1/4	0	0.0000	0.25/0.75	0/0.001(1)	0/0.75
Lattice parameters						
		a (Å)	5.5380(4)	5.3716(2)/3.7651(3)		
		b (Å)	5.5125(3)	5.34022(2)/8.1790(2)		
		c (Å)	8.6680(2)	8.2119(6)/3.7993(4)		
				$\beta = 90.43\ (5)^\circ$ phase fraction (%): 65(ortho.)/35 (mono.)		
$R_p = 13.3$; $R_{wp} = 21.4$; $R_{exp} = 12.43$; $\chi^2 = 2.96$				$R_p = 10.0$; $R_{wp} = 20.5$; $R_{exp} = 12.01$; $\chi^2 = 2.91$		

At ambient conditions, MFeAsF (M = Ca/Sr) crystallizes in the ZrCuSiAs-type structure (space group $P4/nmm$, $Z = 2$). The crystal structures of all the iron-pnictides share a common 2D FeAs layer, where Fe atoms form a 2D-square sublattice with As atoms sitting at the center of these squares but off the Fe plane (above and below the plane alternately). These are made of alternating Ca/SrF and FeAs layers. The Fe and F atoms lie in planes, while the As and Ca/Sr atoms are distributed on each side of these planes following a chessboard pattern. They undergo a tetragonal to orthorhombic phase transition at 134 and 180 K followed by magnetic transitions at 114 and 133 K for CaFeAsF and SrFeAsF, respectively.[22,24] Applications of internal pressure (chemical pressure) suppress both orthorhombic structure and antiferromagnetic state, leading to emergence of superconductivity. For example, the critical superconducting transition temperature $T_c \sim 4$ K in the Co-substituted Fe site in SrFeAsF; $T_c \sim 22$ K in the Co-substituted Fe site in CaFeAsF; and $T_c \sim 31$ K, 52 K, and 56 K, respectively, in the La-, Nd-, and Sm-substituted Sr site in SrFeAsF was observed.[23–28] In addition to this, it was also found that systematically replacing R from La, Ce, Pr, Nd, and Sm in $RFeAsO_{1-\delta}$ resulted in a gradual decreases in the a-axis lattice parameters and an increase in superconducting transition temperature.[23–28,36,37] Superconducting transition temperature (T_c) of different Fe-based superconductors is indeed correlated to their structural properties.[36–40] A systematic trend between T_c and the Fe-As-Fe angles may be expected because the exchange couplings are directly related to the Fe-As-Fe bond angle and Fe-Fe/Fe-As bond distances. It is found that the highest T_c is obtained when the Fe-As-Fe reaches the ideal value of 109.47° for the perfect FeAs tetrahedron with the least lattice distortion.[36–40] This suggests that the most effective way to increase T_c in Fe-based superconductors is to decrease the deviation of the Fe-As-Fe bond angle from the ideal FeAs tetrahedron, as the geometry of the FeAs tetrahedron might be correlated with the density of states near the Fermi energy.

In view of this, we have carried out detailed structural analysis as a function of pressure. Figures 9 and 10 show the pressure dependence of the structural parameters of CaFeAsF and SrFeAsF at 40 K. For easy comparison in Figs. 9–11, we have used converted lattice parameters for the orthorhombic phase ($a = a_o/\sqrt{2}$, $b = b_o/\sqrt{2}$, and $c = c_o$) and for the monoclinic phase ($a = a_m$, $b = b_m$, and $c = c_m$). It is clear from Figs. 9 and 10 that at 40 K on increasing pressure, the lattice parameters monotonically decrease in the entire range of our measurements for CaFeAsF, while the a-lattice parameter of SrFeAsF exhibits anomalous increase beyond

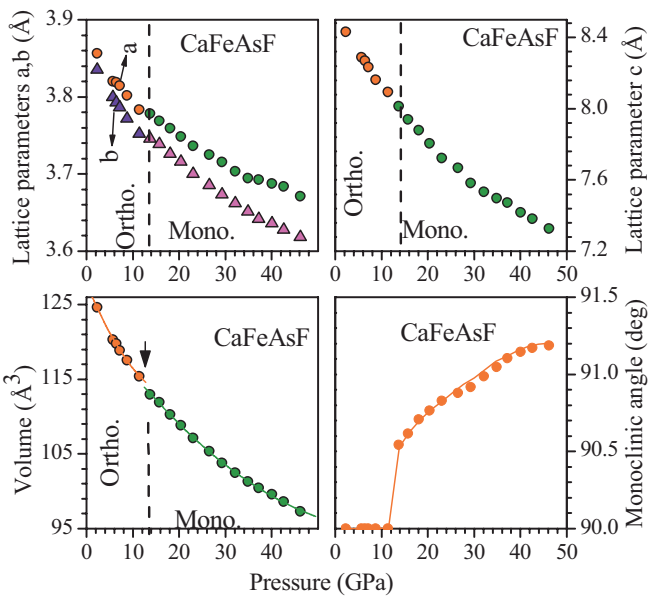

FIG. 9. (Color online) Pressure dependence of the structural parameters (lattice parameters, volume, and monoclinic angle) of CaFeAsF at 40 K as obtained after Rietveld analyses of data with increasing pressure. For the sake of comparison, lattice parameters along [100], [010] and volume of the orthorhombic phase are divided by $\sqrt{2}$ and 2, respectively, and lattice parameters of monoclinic phases are plotted in a standard (cab: $P12/n1$) setting. Errors are within symbol size.

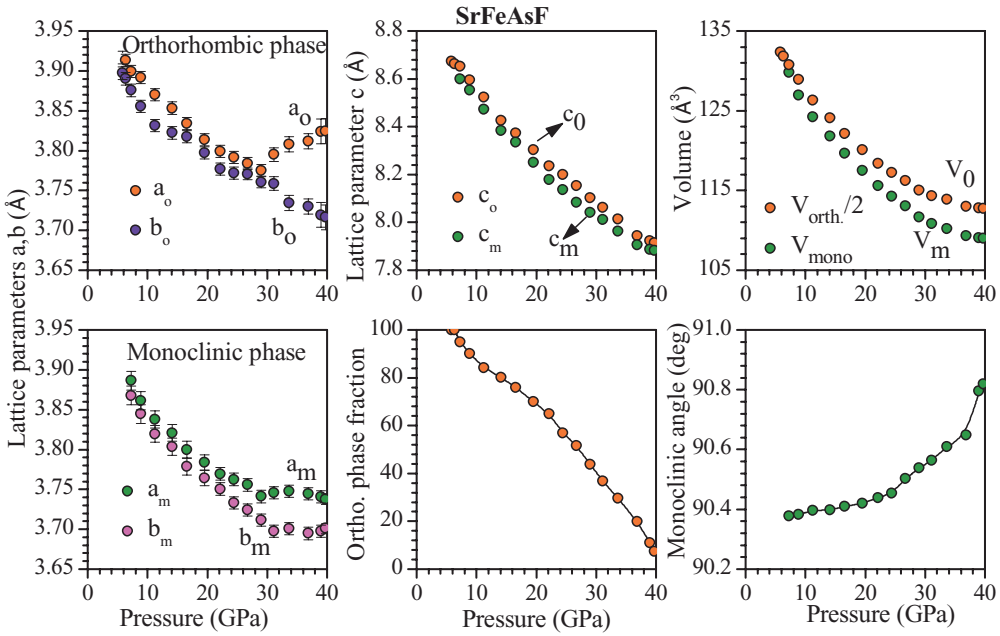

FIG. 10. (Color online) Pressure dependence of the structural parameters (lattice parameters, volume, and monoclinic angle) and orthorhombic phase fraction in SrFeAsF at 40 K as obtained after Rietveld analyses of data with increasing pressure. For the sake of comparison, lattice parameters along [100], [010] and volume of the orthorhombic phase are divided by $\sqrt{2}$ and 2, respectively. Errors are within symbol size.

30 GPa. Figure 11 depicts the pressure evolutions of the normalized lattice parameters, volume, and the ratio $2c/(a+b)$ of CaFeAsF and SrFeAsF compounds at 40 K. It is evident from this figure that the response of the lattice parameters to pressure is strongly anisotropic with the interlayer spacing (along $\langle 001 \rangle$) showing a significantly larger contraction than the basal plane dimensions (along $\langle 100 \rangle$ and $\langle 010 \rangle$). The structural phase transition around 13.7 GPa in the CaFeAsF compound is accompanied by the discontinuity in the pressure evolution of the monoclinic angle (Fig. 9), which clearly suggests a first-order phase transition in CaFeAsF at 13.7 GPa (at 40 K).

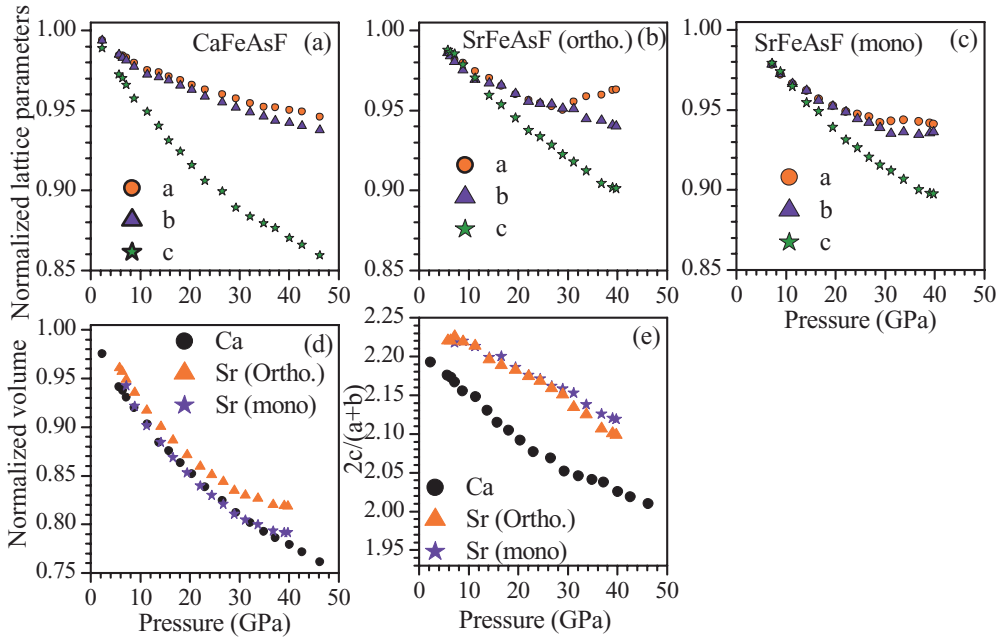

FIG. 11. (Color online) Pressure evolutions of the normalized lattice parameters of (a) CaFeAsF, (b) and (c) SrFeAsF, respectively, at 40 K. Pressure evolutions of the normalized volume and the $2c/(a+b)$ ratio of CaFeAsF and SrFeAsF compounds are shown in (d) and (e). The normalization is done with respect to the ambient pressure values as obtained from a fit to the data of the orthorhombic phase. Errors are within symbol size.

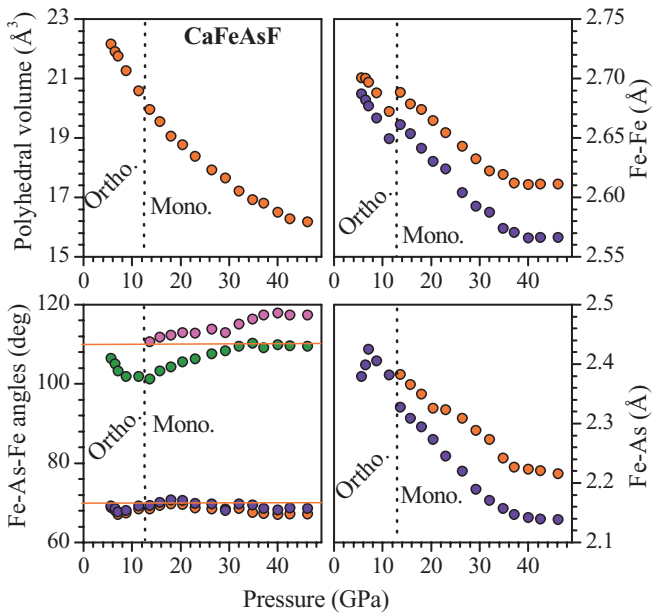

FIG. 12. (Color online) Pressure dependence of the polyhedral volume, Fe-As-Fe bond angle, and Fe-Fe/Fe-As bond length of CaFeAsF at 40 K as obtained after Rietveld analyses of data with increasing pressure. Errors are within symbol size.

The geometry of the $FeAs_4$ tetrahedral units has been identified as a possible control parameter of T_c in the iron pnictides, and it has been argued that it sensitively controls the width of electric conduction band.[5,36,38–40] The pressure variation of $FeAs_4$ polyhedral volume, As-Fe-As bond angle, and Fe-As and Fe-Fe bond lengths obtained from the Rietveld analysis of diffraction data are shown in Figures 12 and 13. It is clear from these figures that the polyhedral volume decreases with increasing pressure. In the case of the CaFeAsF, the Fe-Fe and Fe-As bond lengths reveal anomaly around 11.6 GPa. However, for SrFeAsF, Fe-Fe bond lengths show anomalous increase beyond 30 GPa. A similar anomalous feature in the structural parameters was also observed in $BaFe_2As_2$,[19] which was associated with loss of magnetism. In the present study the angle between As-Fe-As is quite different from the ideal tetrahedral angle of 109.47° and shows anomalous behavior with pressure. It is also evident from Figs. 9–13 that the nature of phase transition seems to be different in CaFeAsF and SrFeAsF. As stated earlier, the transition is sharp in CaFeAsF, whereas SrFeAsF exhibits coexistence of the two phases over a large range of pressure.

Temperature dependence of the electrical resistivity measurements for CaFeAsF at different pressures was carried out by Okada *et al.*[20,21] using the piston-cylinder-type cell and the cubic anvil press. They found that the magnetic transition is suppressed by pressure above 5 GPa, the resistivity anomaly disappears, and superconductivity is observed. Further, the resistivity loss becomes larger, and the superconducting transition shifts to lower temperature with increasing pressure up to 20 GPa. In our experiment, at a fixed temperature of 40 K with increasing pressure, the Fe-As-Fe bond angle decreases over 5 to 10 GPa and then increases with further increasing pressure. Thus, a clear correlation of the bond angle and superconductivity is difficult to establish in view of the different pressure-temperature paths followed in the two experiments. To the best of our knowledge, the high pressure resistivity measurements are still missing for SrFeAsF.

In order to determine the bulk modulus B at zero pressure and its pressure derivative B', the pressure-volume data are fitted by a third-order Birch-Murnaghan equation, and the results are given in Table III. In this table we have also compared the values for several other compounds from literature. The bulk

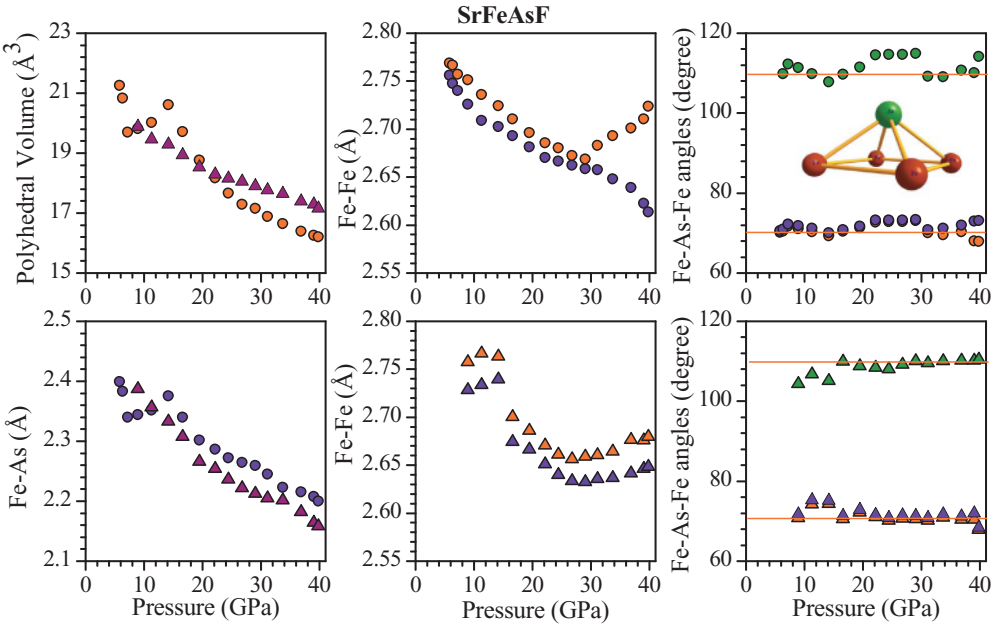

FIG. 13. (Color online) Pressure dependence of the polyhedral volume, As-Fe-As bond angle, and Fe-Fe/Fe-As bond length of SrFeAsF at 40 K as obtained after Rietveld analyses of data with increasing pressure. Solid circle and triangle symbols correspond to the orthorhombic and monoclinic phases, respectively. Errors are within symbol size.

TABLE III. Comparison of the bulk modulus (B) and its pressure derivative (B') of various Fe-based compounds. The standard errors of the fit are given in brackets. In case of the orthorhombic phase of CaFeAsF, the fit resulted in large error bar in pressure derivative (B'), and so it has been fixed at 4.0. The bulk modulus of monoclinic phase of CaFeAsF has been fitted with a fixed value of B' at 4.0 and also with varying B', with the $\chi^2 = 0.6532$ and 0.3569, respectively, which is significantly lower in the latter case.

Compound	Temperature (K)	Bulk modulus at $P = 0$ (GPa)	Pressure derivative of bulk modulus	Pressure range (GPa)	Phase	Reference
CaFeAsF	40	89.4(1.1)	4.0(fixed)	5.8–11.7	Orthorhombic	Present study
	40	135.2(3.4)	3.2(0.2)	13.7–46.0	Monoclinic	Present study
		124.1(0.9)	4.0(fixed)			
	300	107.7(3.5)	2.5(0.3)	13–25	Tetragonal	Present study
SrFeAsF	40	111.1(5.3)	4.0(0.5)	5.8–31.2	Orthorhombic	Present study
	40	114.2(7.3)	4.0(0.6)	11.3-36.3	Monoclinic	Present study
$SmFeAsO_{0.81}F_{0.19}$	300	88.9(0.8)	4.2(0.1)	0–20	Tetragonal	38
$LaFeAsO_{0.9}F_{0.1}$	300	78.0(2.0)	7.4(0.2)	0–32.26	Tetragonal	39
$Fe_{1.03}Se_{0.57}Te_{0.43}$	14	36.6(0.6)	7.8(0.3)	0–9.8	Monoclinic	35
FeSe	16	30.7(1.1)	6.7(0.6)	0–7.5	Orthorhombic	35
$BaFe_2As_2$	300	65.7(0.8)	3.9(0.1)	0–20	Tetragonal	19
	300	153.1(3.0)	1.8(0.1)	32–56	Collapsed tetragonal	19
	40	82.9(1.4)	3.4(0.1)	1–35	Orthorhombic	19
$CaFe_2As_2$	300	74.8(1.2)	4.8(0.1)	4.5–56	Collapsed tetragonal	19
	40	80.2(3.4)	5.4(0.2)	4–34	Collapsed tetragonal	19

modulus in the high-pressure monoclinic phases of CaFeAsF appears larger than that in the orthorhombic phase. However, the values of the bulk moduli for the two phases of SrFeAsF are quite similar. The B values of tetragonal $SmFeAsO_{0.81}F_{0.19}$[38] and $LaFeAsO_{0.9}F_{0.1}$[39] are somewhat lower than those of CaFeAsF and SrFeAsF. The bulk modulus values of other materials such as FeSe and $Fe_{1.03}Se_{0.57}Te_{0.43}$ are much smaller than those of FeAs compounds.

D. Phase transition of CaFeAsF on heating at high pressure

Due to experimental limitations, we could not increase pressure on CaFeAsF beyond 46 GPa at 40 K. However, to see the effect of temperature on the newly stabilized monoclinic phase in CaFeAsF (at 40 K and around 40 GPa), we carried out measurements at different conditions (temperature-pressure), as shown in Fig. 1. Careful analysis of the diffraction data show that there is an abrupt change in the diffraction pattern at 25 GPa and 200 K when the monoclinic splitting/broadening in Bragg reflections around 11.5° and 16.5° disappears (insets of Fig. 14). Detailed Rietveld analyses of the diffraction data reveal that the sample undergoes a structural phase transition from monoclinic to tetragonal phase around 25 GPa and 200 K. It remains in the tetragonal phase at 25 GPa and 300 K. We note that while a phase transition is observed with pressure at 40 K, no transition is found at 300 K. In the case of $SmFeAsO_{0.81}F_{0.19}$ and $LaFeAsO_{0.9}F_{0.1}$[38,39] no phase transition is also found at 300 K up to 20 and 32 GPa, respectively. The fit between the observed and calculated profiles is shown in Fig. 14. For SrFeAsF we have not measured any data point while decreasing the pressure and increasing of temperature. Using a third-order Birch-Murnaghan equation, the fitted values of the bulk modulus B and its pressure derivative B' for CaFeAsF at room temperature are 107.7 ± 3.5 GPa and $B' = 2.5 \pm 0.3$, respectively, as given in Table III.

We have summarized our observations of various phases in CaFeAsF and SrFeAsF with pressure and temperature in Fig. 1. It is interesting to note that at 40 K, CaFeAsF shows orthorhombic to monoclinic phase transition at P_c = 13.7 GPa, whereas at room temperature tetragonal phase is stable up to 25 GPa. The observation of $dP_c/dT > 0$ is similar to that observed in $CaFe_2As_2$ where collapsed

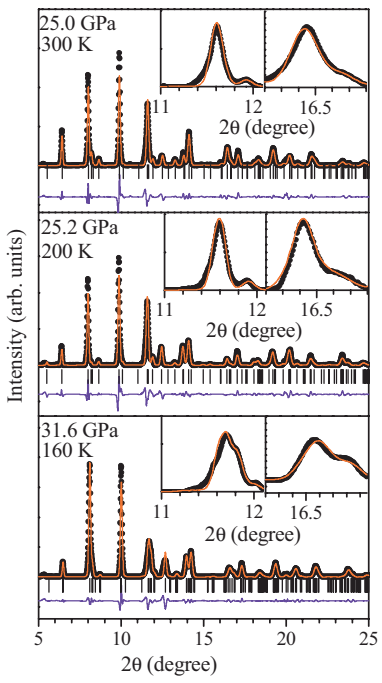

FIG. 14. (Color online) Observed (solid black circles), calculated (continuous red/dark gray line), and difference (bottom blue/medium gray line) profiles obtained after the Rietveld refinement of CaFeAsF at selected pressures and temperature. The diffraction profiles at 31.6 GPa and 160 K are refined using the monoclinic structure (space group $P2/n$); other refinements at 25.2 GPa and 200 K and 25.0 GPa and 300 K are used in tetragonal structure (space group $P4/nmm$). Insets show accountability of certain Bragg's reflections.

tetragonal phase transition occurs at a lower pressure (0.3 GPa) at a low temperature (50 K) in comparison to 1.7 GPa at 300 K. However, this behavior of dP_c/dT may not hold for Ba/Sr compounds.[19] In addition to this, the transition to a lower symmetry phase (orthorhombic to monoclinic) in 1111 (CaFeAsF/SrFeAsF) compound under pressure is in contrast with the high symmetry phase (orthorhombic to tetragonal) in 122 ($BaFe_2As_2$/$CaFe_2As_2$)-type compounds.

IV. CONCLUSION

We have investigated the effect of pressure on the crystal structure and structural phase transition behavior at 40 K in CaFeAsF and SrFeAsF using powder-synchrotron x-ray diffraction and Rietveld analysis technique. We found that both the compounds undergo structural phase transition from orthorhombic to monoclinic phase with increasing pressure. CaFeAsF undergoes a fairly sharp orthorhombic to monoclinic phase transition at 13.7 GPa with increasing pressure. On the other hand, SrFeAsF exhibits coexistence of orthorhombic and monoclinic phases over a large pressure range from 9 to 39 GPa. The coexistence of the two phases indicates that the transition is of first order. On heating from 40 K at high pressure, CaFeAsF undergoes monoclinic to tetragonal phase transition around 25 GPa and 200 K. Further, it does not show any post-tetragonal phase transition up to 25 GPa at 300 K. We note that the 1111-compound (CaFeAsF) undergoes phase transition to a lower symmetry phase (i.e., orthorhombic to monoclinic) under pressure, in contrast with the transition to a higher symmetry phase (i.e., orthorhombic to tetragonal) observed in 122-type compounds ($BaFe_2As_2$ and $CaFe_2As_2$). We have also determined the bulk modulii in these compounds that confirm their soft nature analogous to other compounds in the FeAs family.

ACKNOWLEDGMENTS

R. Mittal and S. K. Mishra thank the Department of Science and Technology (DST), India for providing financial support to carry out synchrotron x-ray diffraction at the European Synchrotron Radiation Facility, Grenoble, France.

*rmittal@barc.gov.in

[1] Y. Izyumov and E. Kurmaev, *High-Tc Superconductors Based on FeAs Compounds,* (Springer, Verlag, Hamburg, 2010); J. S. Schilling, in *Handbook of High Temperature Superconductivity: Theory and Experiments*, edited by J. R. Schrieffer and J. S. Brooks (Spinger Verlag, Hamburg, 2007); H. Takashi and N. Mori, in *Studies of High Temperature Superconductors*, edited by A. Narlikar (Nova Science, New York, 1996).

[2] J. Paglion and R. L. Greene, Nat. Phys. **6**, 645 (2010).

[3] I. I. Mazin and M. D. Johannes, Nat. Phys. **5**, 141 (2009); G. Yu, Y. Li, E. M. Motoyama, and M. Greven, *ibid.* **5**, 873 (2009).

[4] F. Wang and D.-H. Lee, Science **332**, 200 (2011).

[5] J. Zhao, Q. Huang, C. D. Cruz, S. Li, J. W. Lynn, Y. Chen, M. A. Green, G. F. Chen, G. Li, Z. Li, J. L. Luo, N. L. Wang, and P. Dai, Nature Materials **7**, 953 (2008).

[6] C. de la Cruz, Q. Huang, J. W. Lynn, J. Li, W. Ratcliff II, J. L. Zarestky, H. A. Mook, G. F. Chen, J. L. Luo, N. L. Wang, and P. Dai1, Nature (London) **453**, 899 (2008).

[7] I. I. Mazin, D. J. Singh, M. D. Johannes, and M. H. Du, Phys. Rev. Lett. **101**, 057003 (2008); T. Yildirim, *ibid.* **101**, 057010 (2008); C. Feng, H. Yao, W. F. Tsai, J. P. Hu, and S. A. Kivelson, Phys. Rev. B **77**, 224509 (2009).

[8] Y. Kamihara, T. Watanabe, M. Hirano, and H. Hosono, J. Am. Chem. Soc. **130**, 3296 (2008).

[9] K. Ishida, Y. Nakaii, and H. Hosono, J. Phys. Soc. Jpn **78**, 062001 (2009); T. Imai, K. Ahilan, F. L. Ning, T. M. McQueen, and R. J. Cava, Phys. Rev. Lett. **102**, 177005 (2009).

[10] X. H. Chen, T. Wu, G. Wu, R. H. Liu, H. Chen, and D. F. Fang, Nature (London) **453**, 761 (2008).

[11] M. Rotter, M. Tegel, and D. Johrendt, Phys. Rev. Lett. **101**, 107006 (2008).

[12] R. Mittal, L. Pintschovius, D. Lamago, R. Heid, K.-P. Bohnen, D. Reznik, S. L. Chaplot, Y. Su, N. Kumar, S. K. Dhar, A. Thamizhavel, and Th. Brueckel, Phys. Rev. Lett. **102**, 217001 (2009).

[13] R. Mittal, Y. Su, S. Rols, M. Tegel, S. L. Chaplot, H. Schober, T. Chatterji, D. Johrendt, and Th. Brueckel, Phys. Rev. B **78**, 224518 (2008).

[14] H. Takahashi, K. Igawa, K. Arii, Y. Kamihara, M. Hirano, and H. Hosono, Nature (London) **453**, 376 (2008).

[15] M. S. Torikachvili, S. L. Bud'ko, N. Ni, and P. C. Canfield, Phys. Rev. Lett. **101**, 057006 (2008).

[16] T. Park, E. Park, H. Lee, T. Klimczuk, E. D. Bauer, F. Ronning, and J. D. Thompson, J. Phys.: Condens. Matter **20**, 322204 (2008); P. L. Alireza, Y. T. Chris Ko, J. Gillett, C. M. Petrone, J. M. Cole, G. G. Lonzarich, and S. E. Sebastian, J. Phys.: Condens. Matter **21**, 012208 (2009).

[17] C. F. Miclea, M. Nicklas, H. S. Jeevan, D. Kasinathan, Z. Hossain, H. Rosner, P. Gegenwart, C. Geibel, and F. Steglich, Phys. Rev. B **79**, 212509 (2009); T. Terashima, M. Kimata, H. Satsukawa, A. Harada, K. Hazama, S. Uji, H. S. Suzuki, T. Matsumoto, and K. Murata, J. Phys. Soc. Jpn. **78**, 083701 (2009).

[18] H. Okada, K. Igawa, H. Takahashi, Y. Kamihara, M. Hirano, H. Hosono, K. Matsubayashi, and Y. Uwatoko, J. Phys. Soc. Jpn. **77**, 113712 (2008).

[19] R. Mittal, S. K. Mishra, S. L. Chaplot, S. V. Ovsyannikov, E. Greenberg, D. M. Trots, L. Dubrovinsky, Y. Su, Th. Brueckel, S. Matsuishi, H. Hosono, and G. Garbarino, Phys. Rev B **83**, 054503 (2011) and references therein.

[20] H. Okada, H. Takahashi, S. Matsuishi, M. Hirano, H. Hosono, K. Matsubayashi, Y. Uwatoko, and H. Takahashi, Phys. Rev. B **81**, 054507 (2010).

[21] H. Okada, H. Takahashi, H. Takahashi, S. Matsuishi, M. Hirano, and H. Hosono, J. of Phys.: Confer. Series **200**, 012151 (2010).

[22] Y. Xiao, Y. Su, R. Mittal, T. Chatterji, T. Hansen, C. M. N. Kumar, S. Matsuishi, H. Hososno, and Th. Brueckel, Phys. Rev. B **79**, 060504(R) (2009).

[23]T. Hanna, Y. Muraba, S. Matsuishi, K. Kodama, S.-i. Shamoto, and H. Hosono, Phys. Rev. B **84**, 024521 (2011).
[24]Y. Xiao, Y. Su, R. Mittal, T. Chatterji, T. Hansen, S. Price, C. M. N. Kumar, J. Persson, S. Matsuishi, Y. Inoue, H. Hososno, and Th. Brueckel, Phys. Rev. B **81**, 094523 (2010).
[25]S. Matsuishi, Y. Inoue, T. Nomura, H. Yanagi, M. Hirano, and H. Hosono, J. Am. Chem. Soc. **130**, 14428 (2008).
[26]T. Nomura, Y. Inoue, S. Matsuishi, M. Hirano, J. E. Kim, K. Kato, M. Takata, and H. Hosono, Supercond. Sci. Technol. **22**, 055016 (2009).
[27]G. Wu, Y. L. Xie, H. Chen, M. Zhong, R. H. Liu, B. C. Shi, Q. J. Li, X. F. Wang, T. Wu, Y. J. Yan, J. J. Ying, and X. H. Chen, J. of Phys: Conden. Matter **21**, 142203 (2009); L.-F. Zhu and B.-G. Liu, Euro Phys. Lett. **85**, 67009 (2009).
[28]X. Zhu, F. Han, P. Cheng, G. Mu, B. Shen, and H.-H. Wen, Euro Phys. Lett. **85**, 17011 (2009); P. Cheng, B. Shen, G. Mu, X. Zhu, F. Han, B. Zeng, and H.-H. Wen, Europhys. Lett. **85**, 67003 (2009).
[29]S. D. Wilson, Z. Yamani, C. R. Rotundu, B. Freelon, E. Bourret-Courchesne, and R. J. Birgeneau, Phys. Rev. B **79**, 184519 (2009); J.-Q. Yan, A. Kreyssig, S. Nandi, N. Ni, S. L. Bud'ko, A. Kracher, R. J. McQueeney, R. W. McCallum, T. A. Lograsso, A. I. Goldman, and P. C. Canfield, *ibid.* **78**, 024516 (2008).
[30]A. I. Goldman, D. N. Argyriou, B. Ouladdiaf, T. Chatterji, A. Kreyssig, S. Nandi, N. Ni, S. L. Bud'ko, P. C. Canfield, and R. J. McQueeney, Phys. Rev. B **78**, 100506(R) (2008); Y. Xiao, Y. Su, M. Meven, R. Mittal, C. M. N. Kumar, T. Chatterji, S. Price, J. Persson, N. Kumar, S. K. Dhar, A. Thamizhavel, and Th. Brueckel, *ibid.* **80**, 174424 (2009).
[31]A. P. Hammersley, Report No. EXP/AH/95-01 (1995).
[32]J. Rodriguez-Carvajal, Physica B **192**, 55 (1992).
[33]N. Tateiwa and Y. Haga, Rev. Sci. Instrum. **80**, 123901 (2009).
[34]W. Bao, Y. Qiu, Q. Huang, M. A. Green, P. Zajdel, M. R. Fitzsimmons, M. Zhernenkov, S. Chang, M. Fang, B. Qian, E. K. Vehstedt, J. Yang, H. M. Pham, L. Spinu, and Z. Q. Mao, Phys. Rev. Lett. **102**, 247001 (2009).
[35]N. C. Gresty, Y. Takabayashi, A. Y. Ganin, M. T. McDonald, J. B. Claridge, D. Giap, Y. Mizuguchi, Y. Takano, T. Kagayama, Y. Ohishi, M. Takata, M. J. Rosseinsky, S. Margadonna, and K. Prassides, J. Am. Chem. Soc. **131**, 16944 (2009); S. Margadonna, Y. Takabayashi, Y. Ohishi, Y. Mizuguchi, Y. Takano, T. Kagayama, T. Nakagawa, M. Takata, and K. Prassides, Phys. Rev. B **80**, 064506 (2009).
[36]Clarina de la Cruz, W. Z. Hu, Shiliang Li, Q. Huang, J. W. Lynn, M. A. Green, G. F. Chen, N. L. Wang, H. A. Mook, Qimiao Si, and Pengcheng Dai, Phys. Rev. Lett. **104**, 017204 (2010).
[37]C. R. Rotundu, D. T. Keane, B. Freelon, S. D. Wilson, A. Kim, P. N. Valdivia, E. Bourret-Courchesne, and R. J. Birgeneau, Phys. Rev. B **80**, 144517 (2009) and references therein.
[38]G. Garbarino, R. Weht, A. Sow, A. Sulpice, P. Toulemonde, M. Álvarez-Murga, P. Strobel, P. Bouvier, M. Mezouar, and M. Núñez-Regueiro, Phys. Rev. B **84**, 024510 (2011).
[39]G. Garbarino, P. Toulemonde, M. Álvarez-Murga, A. Sow, M. Mezouar, and M. Núñez-Regueiro, Phys. Rev. B **78**, 100507 (2008).
[40]K. Horigane, H. Hiraka, and K. Ohoyama, J. Phys. Soc. Jpn **78**, 074718 (2009).